Reciprocity Evaluation in Heterogeneous Polarimetric SAR Images

Luca Pallotta, *Senior Member, IEEE*

***Abstract*—In this letter, an automatic method to validate the reciprocity theorem on full-polarimetric heterogeneous SAR data is derived. The study extends, to the more general heterogeneous scenario, the work of [1], where the conformity with the reciprocity is studied in the homogeneous case. At the design stage, it is assumed that the pixels in the polarimetric image share the same covariance structure but different power levels. Then, the dependence on nuisance parameters is removed resorting to the Principle of Invariance. The resulting problem is formalized as a binary hypothesis test and is solved through the generalized likelihood ratio test (GLRT). Tests are conducted both on simulated and real-recorded data to show the superiority of the proposed GLRT with respect to its homogeneous counterpart.**

***Index Terms*—Polarimetric SAR, reciprocity, covariance matrix, heterogeneous environment, compound-Gaussian.**

I. Introduction

Polarimetry is undoubtedly among the hottest research topics of the last years, which continuously find application in several contexts regarding synthetic aperture radar (SAR) processing. As a matter of fact, many works, which essentially exploit the polarimetric information to complete the understanding of the observed scene, are continuously published [2]–[10]. However, in spite of the availability of all the polarimetric channels (viz., S_{HH}, S_{VV}, S_{HV}, and S_{VH}), in the majority of data elaborations, a calibration on the reference image is applied to reduce the mismatching effects between HV and VH channels [11]. More precisely, the full-polarimetric image is somehow reduced to three channels by fusing together the HV and VH, for instance, substituting them by their coherent average [12]. In fact, during the acquisition campaign, it could happen that some targets/media might produce mismatching due to statistical fluctuations, Faraday rotations [13], or measurement errors related to sensor non-idealities. Therefore, to better understand the impact of these mismatches on the truthfulness of the reciprocity theorem, in [1] a statistical test aimed at establishing if the reciprocity property is valid for the pixels in a polarimetric image is designed. More specifically, the derived problem is formulated as a binary hypothesis test comprising the presence (null-hypothesis) in competition with the absence (alternative-hypothesis) of reciprocity. Then, it is solved resorting to the generalized likelihood ratio test (GLRT). The main limit of the GLRT devised in [1] derives from the fact that, in the presence of variations in the texture or deviations of data from Gaussianity, it could produce false decisions on reciprocity. To overcome this drawback, in this letter, the framework designed in [1] for the homogeneous environment (HO) is extended to the more general heterogeneous environment (HE) [14], in which it is assumed that the polarimetric pixels share the same covariance structure but have different powers. It is worth to highlight here that, the developed framework is important not only for SAR processing but also for polarimetric search radars, therefore it represents a more far-reaching technique. In fact, many works based on the compound-Gaussian model and that do not consider the validity of reciprocity in their developments [15]–[17] could benefit for the obtained results via a preliminary reciprocity test on training data. Now, since in HE the number of unknown parameters is directly related to that of the samples exploited for the statistical inference, an increment in the amount of data does not reflect in an enhancement in the accuracy of the parameters' estimation. To remove this dependence, the Principle of Invariance [18] is used replacing the original data with their maximal invariant statistic (MIS) with respect to power factors. Then, the statistical characterization of the MIS is obtained under the two competing hypotheses together with the maximum likelihood estimates of the involved parameters to derive the corresponding GLRT. The tests have demonstrated the effectiveness of the proposed GLRT on both numerical and real-recorded data.

The letter is organized as follows. In Section II, the problem of reciprocity assessment in heterogeneous polarimetric SAR images is formulated and the corresponding GLRT is derived. In Section III the results of tests conducted on both simulated and measured data are presented and discussed. Concluding remarks are finally given in Section IV.

Notation: boldface lower case are used for vectors $\boldsymbol{a}$ and boldface upper case for matrices $\boldsymbol{A}$. The transpose, conjugate, and conjugate transpose are denoted by $(\cdot)^T$, $(\cdot)^*$, and $(\cdot)^\dagger$, respectively. $\text{tr}\{\cdot\}$ and $\det(\cdot)$ are the trace and the determinant of the square matrix argument, respectively. $\boldsymbol{I}$ indicates the identity matrix, $\mathbf{1}$ is a vector of all 1 entries, and $\mathbf{0}$ is a vector of all 0 entries, whose sizes are determined from the context. The acronym i.i.d. means independent and identically distribution from a statistical point of view. Finally, $j = \sqrt{-1}$ is the imaginary unit.

II. Problem Formulation and GLRT Derivation

A full-polarimetric SAR sensor measures $N = 4$ complex returns collected from four polarimetric channels of the acquired $L \times M$ image. The N returns associated with the same pixel are organized in the order HH, VV, HV, and VH in the vector $\boldsymbol{x}_{l,m}$, $l = 1, \ldots, L$ and $m = 1, \ldots, M$. As a consequence, a 3-D data stack of size $L \times M \times N$ is realized. The polarimetric returns $\boldsymbol{x}_{l,m}$ are assumed to be i.i.d. and modeled

Luca Pallotta is with University of Roma Tre, Engineering Department, via Vito Volterra 62, I-00146 Roma, Italy. E-mail: luca.pallotta@uniroma3.it

as zero-mean circularly symmetric complex Gaussian vectors with covariance matrix $\mu_{l,m}\boldsymbol{M}$, i.e., $\boldsymbol{x}_{l,m} \sim \mathcal{CN}(\boldsymbol{0}, \mu_{l,m}\boldsymbol{M})$. More precisely, differently from [1], in this letter[1], the pixels are assumed to share the same unknown covariance structure, $\boldsymbol{M}$, but possibly different unknown power levels, $\mu_{l,m}$. Under this assumption, the probability density function (pdf) of $\boldsymbol{x}_{l,m}$ is

$$f(\boldsymbol{x}_{l,m}; \mu_{l,m}, \boldsymbol{M}) = \frac{1}{(\pi\mu_{l,m})^N \det(\boldsymbol{M})} \exp\left\{ -\frac{\text{tr}\left[\boldsymbol{M}^{-1}\boldsymbol{x}_{l,m}\boldsymbol{x}_{l,m}^{\dagger}\right]}{\mu_{l,m}} \right\}. \quad (1)$$

For each pixel under test, a rectangular neighborhood $\mathcal{A}$ of size $K = W_1 \times W_2 \geq N$ is extracted and the vectors in it contained are indicated with $\boldsymbol{x}_1, \ldots, \boldsymbol{x}_K$. Therefore, the polarimetric returns $\boldsymbol{x}_k$, $k = 1, \ldots, K$, are characterized by the covariance $\mu_k\boldsymbol{M}_0$ (or $\mu_k\boldsymbol{M}_1$) if the reciprocity property is (or not) valid, with the scaling factors μ_k accounting for different unknown power levels. Now, to distinguish among the validity of the reciprocal property on SAR data, the problem can be formulated as the following binary hypothesis test

$$\begin{cases} H_0 : \boldsymbol{x}_k \sim \mathcal{CN}(\boldsymbol{0}, \mu_k\boldsymbol{M}_0) & \text{(reciprocity)} \\ H_1 : \boldsymbol{x}_k \sim \mathcal{CN}(\boldsymbol{0}, \mu_k\boldsymbol{M}_1) & \text{(non-reciprocity)} \end{cases} \quad (2)$$

Before proceeding further, it is important to note that the number of unknown parameters is an increasing function of the number of data vectors belonging to $\mathcal{A}$ due to the presence of the scaling factors μ_k. In this case, the ratio between the number of unknown parameters and the number of observations K does not tend to zero as $K \to \infty$. To overcome this limitation and to remove the dependence of the cardinality of $\mathcal{A}$ from the number of nuisance parameters, the Principle of Invariance is used [18]. To this end, as in [9], [10], the original data vectors can be replaced with a suitable function of them, namely the MIS, i.e.,

$$\boldsymbol{z}_k = \frac{\boldsymbol{x}_k}{\|\boldsymbol{x}_k\|}, \quad k = 1, \ldots, K. \quad (3)$$

The transformed data vectors, $\boldsymbol{z}_k$, $k = 1, \ldots, K$, are also i.i.d., and their joint pdf is [21]

$$f(\boldsymbol{z}_1, \ldots, \boldsymbol{z}_K; \boldsymbol{M}) = \Xi(N)[\det(\boldsymbol{M})]^{-K} \prod_{k=1}^{K} \left\{ \text{tr}\left(\boldsymbol{M}^{-1}\boldsymbol{S}_k\right) \right\}^{-N}, \quad (4)$$

with $\boldsymbol{S}_k = \boldsymbol{z}_k\boldsymbol{z}_k^{\dagger}$ and $\Xi(N)$ a normalization constant.

As shown in [1], under the H_0 hypothesis, the covariance has the structure

$$\boldsymbol{M}_0 = \begin{pmatrix} \bar{\boldsymbol{M}} & \begin{matrix} \delta & \delta \\ \delta_1 & \delta_1 \end{matrix} \\ \begin{matrix} \delta^* & \delta_1^* \\ \delta^* & \delta_1^* \end{matrix} & \sigma^2\boldsymbol{1}\boldsymbol{1}^{\dagger} \end{pmatrix} + \gamma^2\boldsymbol{I}, \quad (5)$$

with $\bar{\boldsymbol{M}}$ a 2×2 Hermitian positive semidefinite matrix and γ^2 the power level of thermal noise. The first term stems from the observation that under the reciprocity assumption, $S_{\text{HV}} = S_{\text{VH}}$, the covariances satisfy

$$\begin{aligned} \mathbb{E}\left[|S_{\text{HV}}|^2\right] &= \mathbb{E}\left[|S_{\text{VH}}|^2\right] = \mathbb{E}\left[S_{\text{HV}}S_{\text{VH}}^{\dagger}\right] \\ &= \mathbb{E}\left[S_{\text{VH}}S_{\text{HV}}^{\dagger}\right] = \sigma^2, \end{aligned} \quad (6)$$

$$\mathbb{E}\left[S_{\text{HH}}S_{\text{HV}}^{\dagger}\right] = \mathbb{E}\left[S_{\text{HH}}S_{\text{VH}}^{\dagger}\right] = \delta, \quad (7)$$

and

$$\mathbb{E}\left[S_{\text{VV}}S_{\text{HV}}^{\dagger}\right] = \mathbb{E}\left[S_{\text{VV}}S_{\text{VH}}^{\dagger}\right] = \delta_1. \quad (8)$$

Introducing the unitary matrix $\boldsymbol{U}$

$$\boldsymbol{U} = \begin{pmatrix} \boldsymbol{I} & \boldsymbol{0} & \boldsymbol{0} \\ \boldsymbol{0}^T & 1/\sqrt{2} & 1/\sqrt{2} \\ \boldsymbol{0}^T & 1/\sqrt{2} & -1/\sqrt{2} \end{pmatrix}, \quad (9)$$

it is possible to transform $\boldsymbol{M}_0$ in a block diagonal matrix, i.e.,

$$\boldsymbol{U}\boldsymbol{M}_0\boldsymbol{U}^{\dagger} = \begin{pmatrix} \tilde{\boldsymbol{M}} & \boldsymbol{0} \\ \boldsymbol{0}^T & \gamma^2 \end{pmatrix}, \quad (10)$$

where $\tilde{\boldsymbol{M}}$ is a 3×3 Hermitian positive definite matrix.

The GLRT for (2) is given by

$$\frac{\max_{\boldsymbol{M}_1} f(\boldsymbol{z}_1, \ldots, \boldsymbol{z}_K | \boldsymbol{M}_1, H_1)}{\max_{\boldsymbol{M}_0} f(\boldsymbol{z}_1, \ldots, \boldsymbol{z}_K | \boldsymbol{M}_0, H_0)} \underset{H_0}{\overset{H_1}{\gtrless}} \eta, \quad (11)$$

with η a suitable threshold and $f(\boldsymbol{z}_1, \ldots, \boldsymbol{z}_K | \boldsymbol{M}_h, H_h)$ the likelihood under the H_h hypothesis, $h = 0, 1$, given in (4). The expression of the maximum likelihood under H_1 hypothesis can be derived as

$$\begin{aligned} &\max_{\boldsymbol{M}_1} f(\boldsymbol{z}_1, \ldots, \boldsymbol{z}_K | \boldsymbol{M}_1, H_1) \\ &\quad = \max_{\boldsymbol{M}_1} \frac{\Xi(N)}{[\det(\boldsymbol{M}_1)]^K} \prod_{k=1}^{K} \left\{ \text{tr}\left(\boldsymbol{M}_1^{-1}\boldsymbol{S}_k\right) \right\}^{-N} \\ &\quad = \frac{\Xi(N)}{[\det(\hat{\boldsymbol{M}})]^K} \prod_{k=1}^{K} \left\{ \text{tr}\left(\hat{\boldsymbol{M}}^{-1}\boldsymbol{S}_k\right) \right\}^{-N}, \end{aligned} \quad (12)$$

where $\hat{\boldsymbol{M}}$ is a fixed point of [14], [22]

$$\boldsymbol{M} = \frac{N}{K} \sum_{k=1}^{K} \frac{\boldsymbol{S}_k}{\text{tr}\left(\boldsymbol{M}^{-1}\boldsymbol{S}_k\right)}. \quad (13)$$

Under H_0 hypothesis, the maximum likelihood can be cast as

[1]Note that the heterogeneity assumption made in this letter is only one of several possibilities. As a matter of fact, some pixels in the reference window could contain targets returns with different covariance matrix structures [19], [20] (e.g., single scattering from soil, double scattering from a tree trunk and volumetric scattering from vegetation, and so on), that should be accounted at the design stage.

$$\begin{aligned}
&\max_{\boldsymbol{M}_0} f\left(\boldsymbol{z}_1,\ldots,\boldsymbol{z}_K|\boldsymbol{M}_0,H_0\right)\\
&\quad=\max_{\boldsymbol{M}_0}\frac{\Xi(N)}{[\det(\boldsymbol{M}_0)]^K}\prod_{k=1}^{K}\left\{\mathrm{tr}\left(\boldsymbol{M}_0^{-1}\boldsymbol{S}_k\right)\right\}^{-N}\\
&\quad=\max_{\tilde{\boldsymbol{M}},\gamma}\frac{\Xi(N)}{[\det(\tilde{\boldsymbol{M}})]^K\gamma^{2K}}\\
&\qquad\times\prod_{k=1}^{K}\left\{\mathrm{tr}\left(\tilde{\boldsymbol{M}}^{-1}\boldsymbol{S}_{c1,k}\right)+\mathrm{tr}\left(\gamma^2 s_{c2,k}\right)\right\}^{-N}\\
&\quad=\frac{\Xi(N)}{[\det(\hat{\boldsymbol{M}}_{c1})]^K\hat{m}_{c2}^K}\\
&\qquad\times\prod_{k=1}^{K}\left\{\mathrm{tr}\left(\hat{\boldsymbol{M}}_{c1}^{-1}\boldsymbol{S}_{c1,k}\right)+\mathrm{tr}\left(\hat{m}_{c2}s_{c2,k}\right)\right\}^{-N}
\end{aligned}\tag{14}$$

where

$$\boldsymbol{S}_{1,k}=\boldsymbol{U}\boldsymbol{S}_k\boldsymbol{U}^\dagger=\begin{pmatrix}\boldsymbol{S}_{c1,k} & \boldsymbol{w}_k\\ \boldsymbol{w}_k^\dagger & s_{c2,k}\end{pmatrix}$$

and

$$\hat{\boldsymbol{M}}_U=\boldsymbol{U}\hat{\boldsymbol{M}}\boldsymbol{U}^\dagger=\begin{pmatrix}\hat{\boldsymbol{M}}_{c1} & \boldsymbol{w}\\ \boldsymbol{w}^\dagger & \hat{m}_{c2}\end{pmatrix}$$

with $\hat{\boldsymbol{M}}$ a fixed point of (13). Now, the GLRT can be computed as the ratio between (12) and (14), i.e.,

$$\frac{\det(\hat{\boldsymbol{M}}_{c1})\hat{m}_{c2}}{\det(\hat{\boldsymbol{M}})}\underset{H_0}{\overset{H_1}{\gtrless}}\eta,\tag{15}$$

with η a suitable modification of the original threshold. Since $\det(\hat{\boldsymbol{M}})=\det(\hat{\boldsymbol{M}}_U)$ and using the block partitioned matrix determinant expression [23], (15) can be also recast as

$$\begin{aligned}
\frac{\det(\hat{\boldsymbol{M}}_{c1})}{\det(\hat{\boldsymbol{M}})}\hat{m}_{c2}&=\frac{\det(\hat{\boldsymbol{M}}_{c1})\hat{m}_{c2}}{\det(\hat{\boldsymbol{M}}_{c1})\left(\hat{m}_{c2}-\boldsymbol{w}^\dagger\hat{\boldsymbol{M}}_{c1}^{-1}\boldsymbol{w}\right)}\\
&=\frac{\hat{m}_{c2}}{\left(\hat{m}_{c2}-\boldsymbol{w}^\dagger\hat{\boldsymbol{M}}_{c1}^{-1}\boldsymbol{w}\right)}.
\end{aligned}\tag{16}$$

Consequently, the GLRT is given by the following equivalent form

$$\frac{\boldsymbol{w}^\dagger\hat{\boldsymbol{M}}_{c1}^{-1}\boldsymbol{w}}{\hat{m}_{c2}}\underset{H_0}{\overset{H_1}{\gtrless}}\eta,\tag{17}$$

with η a suitable threshold. Finally, it is worth to underline that, even if the functional form of the statistic in (17) is equal to that provided in [1], this test is more robust since it is derived in a more challenging scenario that encloses the HO as a special case (i.e., when $\mu_k=\mu$, $k=1,\ldots,K$).

III. Results

In this section, the performance of the proposed GLRT for the reciprocity assessment in heterogeneous SAR data is evaluated both on simulated and on real-recorded SAR data.

A. Simulated Data

This subsection illustrates numerical results describing the detection probability P_D of the proposed GLRT. Due to the lack of a closed form expression, P_D is evaluated over 10^3 independent Monte Carlo trials, with the threshold set to ensure a nominal false alarm probability $P_{FA}=10^{-4}$. Data are modeled as spherically invariant random vectors (SIRVs) [24], i.e.,

$$\boldsymbol{x}_k=\sqrt{\tau_k}\boldsymbol{g}_k,\quad k=1,\ldots,K,\tag{18}$$

where τ_k is a positive real random variable statistically independent of $\boldsymbol{g}_k$s, which are i.i.d. N-dimensional zero-mean complex circular Gaussian vectors with covariance $\boldsymbol{M}_1=\bar{\boldsymbol{M}}_1+\gamma^2\boldsymbol{I}$. The term $\gamma^2=10^{-3}$ is the actual power level of thermal noise, while $\bar{\boldsymbol{M}}_1$ is a $N\times N$ Hermitian matrix associated with a scene of mixed scrubs [2],

$$\bar{\boldsymbol{M}}_1=0.098\begin{pmatrix}1 & 0.60 & 0 & 0\\ 0.60 & 1.08 & 0 & 0\\ 0 & 0 & 0.19 & 0.19\,(1+\xi)\,e^{-j\phi}\\ 0 & 0 & 0.19\,(1+\xi)\,e^{j\phi} & 0.19\,(1+\xi)^2\end{pmatrix},$$

with ξ a scaling factor modeling modulus variations and ϕ accounting for phase mismatches between the HV and VH channels. Finally, $\tau_1,\ldots,\tau_K$ are i.i.d. and obey the Gamma distribution with pdf

$$f(\tau)=\frac{1}{\Gamma(\nu)}\frac{1}{\mu^\nu}\tau^{\nu-1}e^{-\tau/\mu}u(\tau),$$

where $\Gamma(\cdot)$ is the Eulerian Gamma function, μ and $\nu>0$ are the scale and shape parameters, respectively (the considered setting assumes $\mu=1/\nu$ to have a Gamma distribution with unit mean).

Figure 1 reports P_D versus ξ for some values of the parameter ν of the Gamma distribution for the proposed GLRT in HE (HE-GLRT in the following) also in comparison with its homogeneous counterpart devised in [1] and referred to as HO-GLRT. The subplots are obtained for a) $K=9$ and b) $K=25$ looks, whereas the phase difference among the polarimetric channels HV and VH is chosen to be a uniform random variable $\phi\sim\mathcal{U}[-10^\circ,10^\circ]$. The curves clearly show that for ξ close to 0, the H_0 hypothesis (i.e., reciprocity) is detected, whereas moving away from that value, the H_1 hypothesis (i.e., non-reciprocity) is preferred. In addition, increasing the number of looks K (i.e., from subplot a to b), H_1 selection arises in correspondence of low values of ξ, confirming the effectiveness of the test. It is also evident that the proposed test is able to perform better than the HO-GLRT for low values of ν. However, as the latter increases, the data distribution approaches the Gaussian, with the consequent reduction of the performance gain of the HE-GLRT over the competitor.

B. Real-Recorded Data

This subsection validates reciprocity on the L-band (1.27 GHz) coherent full-polarimetric dataset[2], acquired by the

[2]Data can be downloaded at *https://earth.esa.int/web/polsarpro/data-sources/sample-datasets* [12] thanks to Prof. Yoshio Yamaguchi and CRL Niigata University.

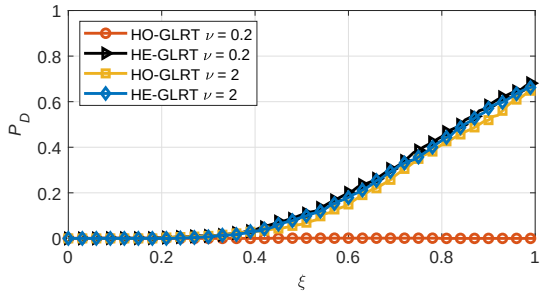

(a)

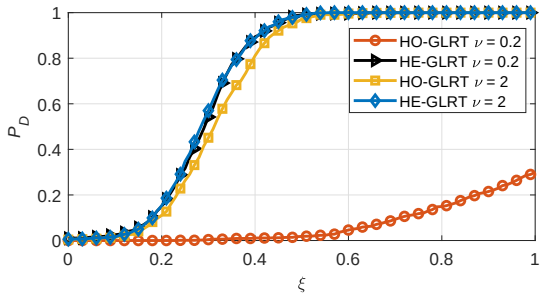

(b)

Figure 1. P_D versus ξ for a random phase variation between the HV and VH channels $\phi \sim \mathcal{U}[-10°, 10°]$, and different number of looks: a) $K = 9$ and b) $K = 25$. The nominal P_{FA} is set to 10^{-4}.

airborne Polarimetric and Interferometric SAR (PiSAR) developed by the Communications Research Laboratory (CRL) of the Ministry of Posts and Telecommunications of Japan and the National Space Development Agency of Japan (NASDA). The image, of size 2000×2000 pixels, represents a scene of the Tsukuba Site Area (JP) acquired with a resolution of 2.5 m, and contains a mixed urban, vegetation and cultivated fields. Figure 2 shows the Pauli decomposition [5] in the Red-Green-Blue (RGB) color space of the Tsukuba PiSAR polarimetric data, its span (i.e., the polarimetric image power $|\text{HH}|^2 + |\text{VV}|^2 + |\text{HV}|^2 + |\text{VH}|^2$), the modulus of the difference between the HV and VH channels, and the results of application of the HO-GLRT and HE-GLRT with a sliding window of size $K = W \times W = 9$ exploiting a threshold set for a nominal $P_{FA} = 10^{-4}$. From the inspection of this result (subplots d-e), it can be claimed that this polarimetric data share the reciprocity property, since the number of detections (i.e., H_1 hypothesis) in the image is very low. In fact, as drawn in Table I, the percentage of pixels that exhibit a reciprocal behavior is equal to 95.81% for the HE-GLRT and 93.70% for the HO-GLRT, respectively (a similar trend can be also observed for $P_{FA} = 10^{-3}$). It is also worth to emphasize the agreement among the detection maps in Figures 2-d) - 2-e) and the $|\text{HV} - \text{VH}|$ values represented in 2-c), with detections corresponding to high values of $|\text{HV} - \text{VH}|$. Comparing Figures 2-b and 2-c, it can be conjectured that, beyond the noise contribution, that is uniformly distributed over the entire images, some miscalibration between the two competing HV and VH images is present, with more evidence in correspondence of high intensity pixels. These differences in the two channels of course produce several detections in the detection maps of Figures 2-d and 2-e. Moreover, it can be observed that texture variations also produce false decisions whose amount is reduced if the proposed GLRT is applied in place its homogeneous counterpart. As a matter of fact, from the detection maps it is also clear that the HE-GLRT gains over the HO-GLRT in correspondence of higher texture values, as highlighted by the circles inside those figures. This is motivated by the fact that the presence of strong textures associated to some pixels within the reference window used to estimate the covariance could produce a severe degradation in the performance of a GLRT designed assuming an homogeneous scenario. From this premise, it can be claimed that the remaining percentage of detection can be explained as due to possible loss of Gaussianity as well as miscalibration of the two channels during the acquisition process (as confirmed by the visual inspection of Fig. 2-c). Before concluding, it is useful to emphasize that miscalibration could be caused by saturation (identified by the white color in Fig. 2-a). In fact, saturation reduces the accuracy in the polarimetric analysis that, in turn, leads to possible miscalibrations (see the areas in the 2 circles in the lower right corner of the figures).

Table I
NUMBER OF ESTIMATED PIXELS (IN PERCENTAGE) COMPLYING WITH RECIPROCITY FOR THE TSUKUBA PISAR DATA OF FIG. 2.

	$P_{FA} = 10^{-3}$		$P_{FA} = 10^{-4}$	
	HO-GLRT	HE-GLRT	HO-GLRT	HE-GLRT
H_0	85.68%	88.70%	93.70%	95.81%
H_1	14.32%	11.29%	6.30%	4.19%

IV. CONCLUSIONS

This letter has devised a new framework aimed at establishing the validity of the reciprocity theorem in real-recorded full-polarimetric heterogeneous data. More precisely, at the design stage, it has been assumed that each pixel has a different power level but the same covariance structure; then original data have been substituted by their MIS to remove dependence on nuisance parameters before deriving the corresponding GLRT. The performance analyses, conducted both on simulated and measured data, have shown the effectiveness of the proposed solution and its advantages with respect to its competitor for homogeneous environments. Possible future works could test the proposed algorithm on images acquired by satellite sensors as well as in higher bandwidths such as X or Ku. Moreover, it would be interesting to consider more-sophisticated models for the heterogeneous environment accounting for different covariance structures arising for the presence of different kinds of targets in the reference window data.

ACKNOWLEDGMENT

The author would like to acknowledge ESA for providing the PiSAR sample data.

The author acknowledges fruitful discussions with Prof. Antonio De Maio of University of Naples “Federico II”.

The author thanks the Associate Editor and Reviewers for the interesting comments that have helped to improve this letter.

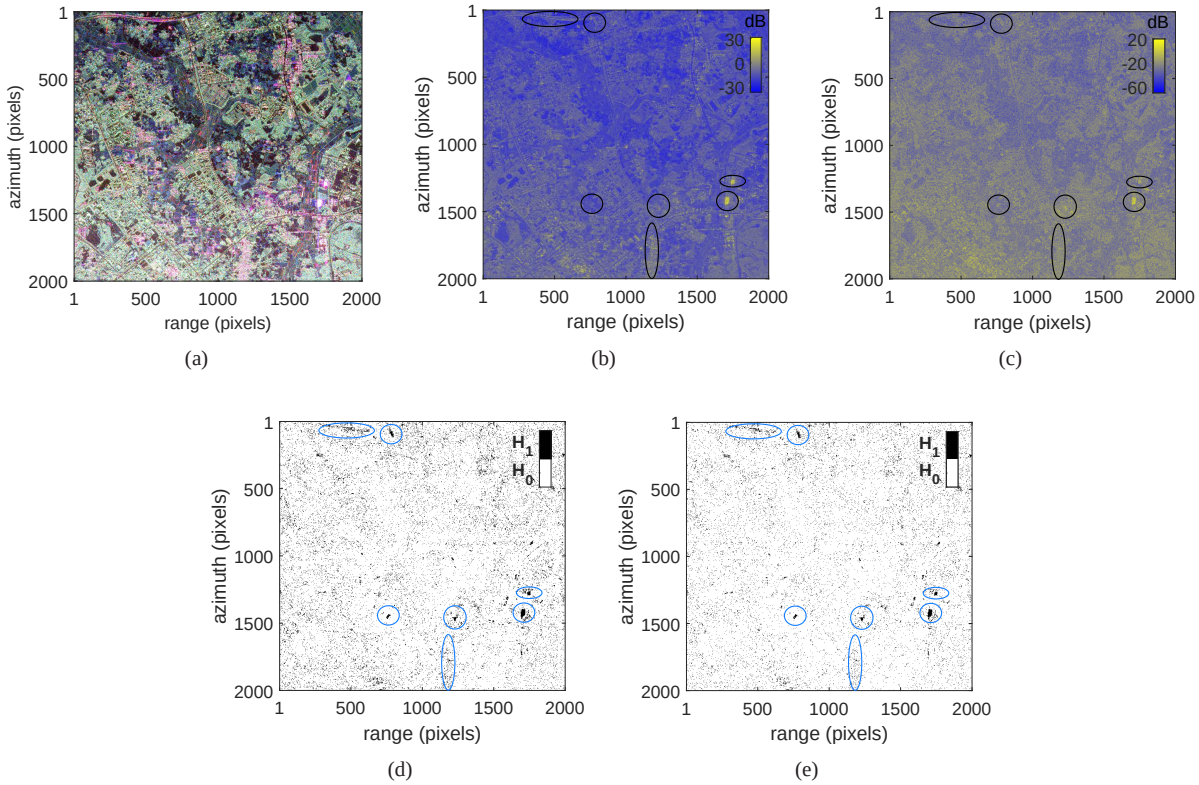

Figure 2. Reciprocity assessment for the L-band PiSAR data of Tsukuba (JP), using $K = 9$ looks. Subplots refer to a) RGB Pauli decomposition, b) span, c) $|\mathrm{HV} - \mathrm{VH}|$ (dB), d) HO-GLRT, and e) HE-GLRT. Threshold is set to have $P_{FA} = 10^{-4}$.

REFERENCES

[1] A. Aubry, V. Carotenuto, A. De Maio, and L. Pallotta, "Assessing Reciprocity in Polarimetric SAR Data," *IEEE Geoscience and Remote Sensing Letters*, vol. 17, no. 1, pp. 87–91, 2019.

[2] L. M. Novak, M. C. Burl, and W. W. Irving, "Optimal Polarimetric Processing for Enhanced Target Detection," *IEEE Trans. on Aerospace and Electronic Systems*, vol. 29, no. 1, pp. 234–244, January 1993.

[3] S. R. Cloude and E. Pottier, "An Entropy Based Classification Scheme for Land Applications of Polarimetric SAR," *IEEE Trans. on Geoscience and Remote Sensing*, vol. 35, no. 1, pp. 68–78, January 1997.

[4] L. Ferro-Famil and E. Pottier (Editor in Chief J. A. Kong), *Progress In Electromagnetics Research*, vol. 24, chapter Dual Frequency Polarimetric SAR Data Classification and Analysis, pp. 251–276, New York Elsevier, 2001.

[5] J. S. Lee and E. Pottier, *Polarimetric Radar Imaging: From Basics to Applications*, CRC Press, 2009.

[6] A. Moreira, P. Prats-Iraola, M. Younis, G. Krieger, I. Hajnsek, and K. P. Papathanassiou, "A Tutorial on Synthetic Aperture Radar," *IEEE Geoscience and Remote Sensing Magazine*, vol. 1, no. 1, pp. 6–43, 2013.

[7] V. Carotenuto, A. De Maio, C. Clemente, and J. J. Soraghan, "Invariant Rules for Multipolarization SAR Change Detection," *IEEE Trans. on Geoscience and Remote Sensing*, vol. 53, no. 6, pp. 3294–3311, 2015.

[8] L. Pallotta, C. Clemente, A. De Maio, and J. J. Soraghan, "Detecting Covariance Symmetries in Polarimetric SAR Images," *IEEE Trans. on Geoscience and Remote Sensing*, vol. 55, no. 1, pp. 80–95, January 2017.

[9] L. Pallotta, A. De Maio, and D. Orlando, "A Robust Framework for Covariance Classification in Heterogeneous Polarimetric SAR Images and its Application to L-Band Data," *IEEE Trans. on Geoscience and Remote Sensing*, vol. 57, no. 1, pp. 104–119, January 2019.

[10] L. Pallotta and D. Orlando, "Polarimetric Covariance Eigenvalues Classification in SAR Images," *IEEE Geoscience and Remote Sensing Letters*, vol. 16, no. 5, pp. 746–750, May 2019.

[11] F. T. Ulaby and D. G. Long, *Microwave Radar and Radiometric Remote Sensing*, University of Michigan Press, 2013.

[12] ESA, "PolSARPro (The Polarimetric SAR Data Processing and Educational Tool)," 2000-2019.

[13] E. J. M. Rignot, "Effect of Faraday Rotation on L-Band Interferometric and Polarimetric Synthetic-Aperture Radar Data," *IEEE Trans. on Geoscience and Remote Sensing*, vol. 38, no. 1, pp. 383–390, January 2000.

[14] G. Vasile, J. P. Ovarlez, F. Pascal, and C. Tison, "Coherency Matrix Estimation of Heterogeneous Clutter in High-Resolution Polarimetric SAR Images," *IEEE Trans. on Geoscience and Remote Sensing*, vol. 48, no. 4, pp. 1809–1826, 2010.

[15] A. De Maio, G. Alfano, and E. Conte, "Polarization Diversity Detection in compound-Gaussian Clutter," *IEEE Transactions on Aerospace and Electronic Systems*, vol. 40, no. 1, pp. 114–131, 2004.

[16] G Alfano, A De Maio, and E Conte, "Polarization Diversity Detection of Distributed Targets in compound-Gaussian Clutter," *IEEE Transactions on Aerospace and Electronic Systems*, vol. 40, no. 2, pp. 755–765, 2004.

[17] E. Conte, A. De Maio, and C. Galdi, "Statistical Analysis of Real Clutter at Different Range Resolutions," *IEEE Transactions on Aerospace and Electronic Systems*, vol. 40, no. 3, pp. 903–918, 2004.

[18] E. L. Lehmann, *Testing Statistical Hypotheses*, Springer-Verlag, New York, USA, 2nd ed. edition, 1986.

[19] S. R. Cloude and E. Pottier, "A Review of Target Decomposition Theorems in Radar Polarimetry," *IEEE Trans. on Geoscience and Remote Sensing*, vol. 34, no. 2, pp. 498–518, March 1996.

[20] T. Eltoft and A. P. Doulgeris, "Model-Based Polarimetric Decomposition with Higher Order Statistics," *IEEE Geoscience and Remote Sensing Letters*, vol. 16, no. 6, pp. 992–996, 2019.

[21] E. Ollila, D. E. Tyler, V. Koivunen, and H. V. Poor, "Complex Elliptically Symmetric Distributions: Survey, New Results and Applications," *IEEE Trans. on Signal Processing*, vol. 60, no. 11, pp. 5597–5625, 2012.

[22] E. Conte, A. De Maio, and G. Ricci, "Recursive Estimation of the Covariance Matrix of a Compound-Gaussian Process and its Application to Adaptive CFAR Detection," *IEEE Transactions on Signal Processing*, vol. 50, no. 8, pp. 1908–1915, 2002.

[23] R. A. Horn and C. R. Johnson, *Matrix Analysis*, Cambridge University Press, 1990.

[24] E. Conte and M. Longo, "Characterisation of Radar Clutter as a Spherically Invariant Random Process," *IEE Proceedings Communications, Radar and Signal Processing*, vol. 134, no. 2, pp. 191–197, April 1987.